Performance and control optimisations using the adaptive torsion wing

R. M. Ajaj **M. I. Friswell** **W. G. Dettmer**
R.M.Ajaj@swansea.ac.uk
College of Engineering
Swansea University
Swansea, UK

G. Allegri
Department of Aerospace Engineering
University of Bristol
Bristol, UK

A. T. Isikveren
Bauhaus Luftfahrt
Munich, Germany

ABSTRACT

This paper presents the Adaptive Torsion Wing (ATW) concept and performs two multidisciplinary design optimisation (MDO) studies by employing this novel concept across the wing of a representative UAV. The ATW concept varies the torsional stiffness of a two-spar wingbox by changing the enclosed area through the relative chordwise positions of the front and rear spar webs. The first study investigates the use of the ATW concept to improve the aerodynamic efficiency (lift-to-drag ratio) of the UAV. In contrast, the second study investigates the use of the concept to replace conventional ailerons and provide roll control. In both studies, the semi-span of the wing is split into five equal partitions and the concept is employed in each of them. The partitions are connected through thick ribs that allow the spar webs of each partition to translate independently of the webs of adjacent partitions and maintain a continuous load path across the wing span. An MDO suite consisting of a Genetic Algorithm (GA) optimiser coupled with a high-end low-fidelity aero-structural model was developed and employed in this paper.

Paper No. 3775. Manuscript received 11 October 2011, revised version received 3 January 2012, accepted 23 February 2012.

NOMENCLATURE

a	lift-curve slope (radian^{-1})
A	enclosed area (m^2)
[**A**]	aerodynamic inertia matrix
[**B**]	aerodynamic damping matrix
c	wing chord (m)
[**C**]	structural damping matrix
D	drag (N)
[**D**]	aerodynamic stiffness matrix
ds	infinitesimal segment along the perimeter of the closed section (m)
{**F**}	Nodal forces and moments vector (N or Nm)
G	shear modulus (N/m^2)
J	torsion constant (m^4)
[**K**]	stiffness matrix
l	wing semi-span (m)
L	lift (N)
L'	unsteady lift per unit span
[**M**]	inertia matrix
$M'o$	unsteady moment on the aerodynamic centre per unit span
L_r	rolling moment (Nm)
t	wall thickness (m)
U	airspeed (ms^{-1})
w	vertical the plunge displacement (positive upward) (m)
W	UAV weight (N)
x	web position as percentage of the wingbox chord (%)
N	yawing moment (Nm)
$\{q\}$	vector of the degrees of freedom (m or radian)
θ	twist angle (radian)

Subscripts

dd	design dive
div	divergence
fr	flutter
fw	front web
rw	rear web

1.0 INTRODUCTION

The idea of modifying the aerodynamic profile of a lifting surface to enhance flight control and aircraft performance is not new. The Wright Brothers employed wing warping as a seamless flight control in their first flying machine. Conventional control surfaces present various limitations on the manoeuvrability and the capability of the air-vehicle; they set different constraints on its flight envelope and mission effectiveness, and increase the installation and maintenance costs of the airframe significantly[1]. For instance, during the design of the Myasishchev M-50 and Tsybin R-020 Russian aircraft, it appeared that using conventional ailerons to provide roll control required

large increase in weight (overdesigning the wings) to prevent aileron reversal problems and to maintain aileron effectiveness at large dynamic pressures[2-4]. This has focused the interests of aircraft designers on adaptive structures that use wing flexibility to augment the performance of conventional control surfaces or replace them. Active Aeroelastic Structures (AAS) are a set of adaptive structures that allows significant performance and control enhancements by manipulating the aerodynamic profile/shape of a lifting surface, without the need for significant platform modifications that typically require complex and heavy mechanisms. AAS depend on the aerodynamic loads to deform them and maintain their shape; this reduces the energy requirements associated with these structures.

Recently, the use of AAS to replace conventional control surfaces, enhance control authority, and enhance stealth characteristics of air-vehicles has been under thorough investigation in a number of research programs and projects across the world. In the United States of America, both the Active Flexible Wing (AFW) program[5] and the Active Aeroelastic Wing (AAW) program[6,7] investigated the use of flexible wing structures coupled with leading and trailing-edge control surfaces. The structural deformations of an advanced fighter wing were manipulated in order to eliminate aileron reversal problems at large dynamic pressures and to maximise the rolling performance according to design intent without using the horizontal tail to augment roll performance. Furthermore, Griffin *et al*[8] investigated the use of a smart spar concept to vary the torsional stiffness and to control the aeroelastic behaviour of a representative wing; this design concept also aimed to enhance the roll rate of high performance aircraft at high dynamic pressures. The solution proposed was based on the simultaneous actuation of control surfaces and the modification of the wing torsional stiffness using the aforementioned smart spar concept. The latter has a web that can either transfer shear between the upper and lower spar caps or disable such load transmission mechanism. This is achieved by allowing the smart spar to move from a reference position along the leading edge to a diagonal arrangement where the front caps at the wing root are connected to the aft most ones at the wing tips. Similarly, Chen *et al*[9] developed the Variable Stiffness Spar (VSS) concept to vary the torsional stiffness of the wing and again enhance the roll performance. Their VSS concept consisted of a segmented spar having articulated joints at the connections with the wing ribs and an electrical actuator capable of rotating the spar through 90 degrees. In the horizontal position, the segments of the spar are uncoupled and the spar offers no bending stiffness. In the vertical position, the segments join completely and the spar provides the maximum torsional and bending stiffness. The concept allows the stiffness and aeroelastic deformations of the wing to be controlled depending on the flight conditions.

Nam *et al*[10] took the VSS solution a step forward and developed the torsion-free wing concept. This aimed to attain a post-reversal aeroelastic amplification of wing twist. The primary structure of the torsion free wing consists of two main parts. The first is a narrow wingbox tightly attached to the upper and lower wing skin in order to provide the basic wing torsional stiffness. The second part consists of two variable stiffness spars placed near the leading and trailing edges, passing through all of the rib holes. Nam *et al*. demonstrated that the torsion-free wing can provide significant aeroelastic amplification, leading to an increase in roll-rate between 8% and 48 % over the baseline performance in the worst possible flight conditions. Florance *et al*[11] investigated the use of the VSS concept to exploit the wing flexibility and to improve the aerodynamic performance of the vehicle. Their wing incorporated a spar with a rectangular cross-section that runs from the wing root up to 58% of the overall wing semi-span. The spar is used to change the wing bending and torsional stiffness as it rotates between vertical and horizontal positions.

In Europe, the Active Aeroelastic Aircraft Structures (3AS) research project[2-4] which involved a consortium of 15 European partners in the aerospace industry and was partially funded

by the European Community, focused on developing active aeroelastic design concepts through exploiting structural flexibility in a beneficial manner. The final aim was to improve the aircraft aerodynamic efficiency. One of the novel concepts proposed was the All-Moving Vertical Tail (AMVT) with a variable torsional stiffness attachment[12,13]. The AMVT concept achieved a smaller and lighter fin while maintaining stability and rudder effectiveness for a wide range of airspeeds. The AMVT employs a single attachment and the position of the attachment can be adjusted in the chord-wise direction relative to the position of the centre of pressure to achieve aeroelastic effectiveness above unity[12]. Furthermore, the 3AS project investigated a variety of variable stiffness attachments and mechanisms for the AMVT concept including a pneumatic device developed at the University of Manchester[13]. As part of the 3AS project, Cooper *et al*[14-16] investigated two active aeroelastic structure concepts that modify the static aeroelastic twist of the wing by modifying its internal structure. The first concept exploited the chord-wise translation of an intermediate spar in a three spars wingbox in order to vary its torsional stiffness and the position of the shear centre. The second concept was similar to the VSS concept where rotating spars are employed to vary the torsional and bending stiffness as well as the shear centre positions. Prototypes of such concepts were built and tested in the wind tunnel to examine their behaviour under aerodynamic loadings.

This paper presents the adaptive torsion wing (ATW) concept, which facilitates targeted aeroelastic twist deformations of the structure in a beneficial manner, and performs preliminary Multidisciplinary Design Optimisation (MDO) studies by employing this novel concept across the wing of a UAV. The ATW concept modifies the torsional stiffness of a thin-walled, closed section, two-spar wingbox by changing the area enclosed between the front and rear spar webs[17,18]. The enclosed area is modified by translating the spar webs in the chord-wise direction towards each other using internal actuators, as shown Fig.1. The objectives of these studies are to assess the effectiveness of the ATW as a roll control device and to assess the performance benefits (lift to drag ratio) that can be achieved with this concept. Each semi-span of the UAV's wing is split into equal five partitions from root to tip, and the ATW concept is employed within each partition. At the ends of each partition, there are thick connecting ribs that allow the spar webs of each partition to translate independently of the webs of the adjacent partitions. Furthermore, the thick ribs transfer the shear loads between the webs of adjacent partitions and between the webs and the equivalent skins (covers and stringers) to maintain a closed wingbox section and a continuous load path across the various components of the wingbox. The MDO suite consisting of the Genetic Algorithm (GA) optimiser coupled with a high-end low-fidelity aero-structural model[19,20] was developed in MATLAB™.

2.0 THE ADAPTIVE TORSION WING (ATW)

The ATW concept is a thin-walled closed section wingbox (Fig. 1(a)) whose torsional stiffness can be adjusted through the relative position of the front and rear spar webs. The torsional stiffness (*GJ*) for a thin-walled closed section can be estimated from the 2nd Bredt-Batho equation as:

$$GJ = \frac{4GA^2}{\oint \frac{ds}{t}} \qquad \ldots (1)$$

where G is the shear modulus, J is the torsion constant, A is the enclosed area, t is the wall thickness, and ds is an infinitesimal segment along the perimeter. If a single material is used in

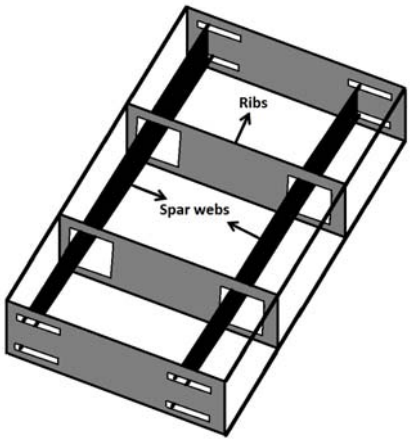

(a) The adaptive torsion wingbox

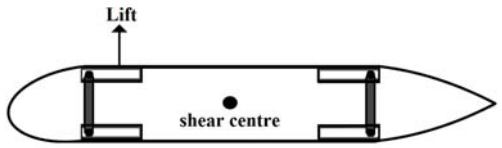

(b) Maximum torsional stiffness web positions

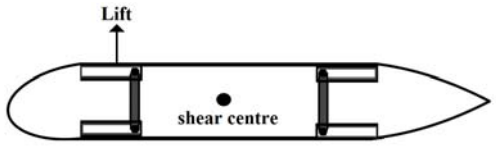

(c) Minimum torsional stiffness web positions

Figure 1. A conceptual sketch of the Adaptive Torsion Wing concept.

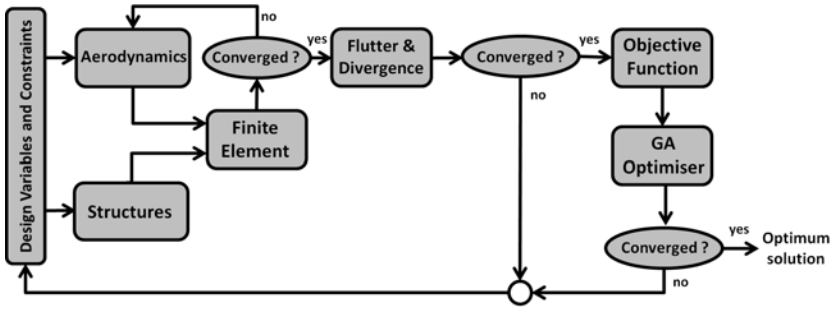

Figure 2. Flowchart and relational diagram of the MDO Suite.

the wingbox, the resulting torsional stiffness only depends on the square of the enclosed area; therefore the torsional stiffness of the section can be altered by varying the position of the front spar web, the rear spar web, or both, to change the enclosed area, as shown in Fig. 1. The change in web positions (Figure 1(b) and 1(c)), results in two components of torsional stiffness, the first component is due to the closed section while the second comes from the skin/web segments belonging to the open section(s). The analysis in this paper accounts only for the closed-section component, because the torsional stiffness associated with the open section segments is several orders of magnitude smaller.

3.0 THE MDO SUITE

The MDO suite[19,20] belongs to the family of high-end, low-fidelity optimisation tools. It consists of a Genetic Algorithm (GA) optimiser coupled with the Tornado Vortex Lattice Method (TVLM), a Structural model, a Finite Element (FE) model, and flutter and divergence checks, as shown in Fig. 2.

3.1 Genetic Algorithm (GA) optimiser

Genetic Algorithms (GAs) are stochastic global search and optimisation methods. GAs mimic the metaphor of natural evolution by applying the principle of the survival of the fittest to produce successively better approximations to a solution[21]. They follow a population-based approach which allows the optimisation process to be parallelised and hence to reduce the computational time. GAs start with an initial population consisting of various individuals, and each individual represents a particular solution to the problem. The population evolves over generations to produce better solutions. The 'Matlab GA Toolbox', developed by Chipperfield *et al*[22], was incorporated in this analysis. A fitness value is assigned to every individual of the initial population through an objective function that assesses the performance of the individual in the problem domain. Then, individuals are selected based on their fitness index and crossover between them is performed to generate new offspring. Finally, mutation of the new offspring is performed to ensure that the probability of searching any subspace of the problem is never zero[21]. These abovementioned processes iterate until the optimum solution is achieved depending on the convergence criteria of the problem.

3.2 Aerodynamics

The Tornado Vortex Lattice Method (TVLM)[23] was used for the aerodynamic predictions. Tornado is a linear aerodynamics code, and thus it discounts wing thickness and viscous effects. These limitations imply that Tornado can only be used for angles of attack up to 8-10° for slender wings. Linear aerodynamic theory is still nevertheless very useful as most aircraft typically operate within the linear region (operating lift coefficients at reference speeds) in cruise, as well as both take-off and landing phases. These are the flight stages in which this research and analysis has been undertaken. The representative UAV considered is similar to the BAE Systems Herti UAV. Figure 3 shows the wing and empennage built in Tornado. A convergence study was undertaken to select the optimum spanwise mesh. This study shows that 10 spanwise panels are enough to model the aerodynamic loads on the wing when the aeroelastic deformations are neglected. However, the convergence study showed that 60 spanwise panels are required to model the aerodynamic loads when aeroelastic deformations are considered, yielding an error of 0·5% in the lift force. Therefore, in this analysis, 4 chordwise panels and 60 spanwise panels with a cosine distribution are used per wing semi-span. The fuselage contribution to parasitic drag is accounted for by assuming an equivalent cylinder model. The UAV has a rectangular, unswept, untwisted wing. The specifications of the UAV are listed in Table 1.

Table 1
The UAV's specifications

UAV specifications	Values
wing area	22·44m^2
MTOW	800kg
aerofoil	NACA 4415
maximum cruise speed	65ms^{-1}
design dive speed	≈ 82ms^{-1}
span	12m
chord	1·87m
wing loading	35·70kg/m^2

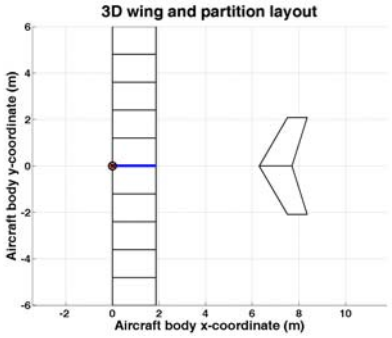

Figure 3. The geometry of the UAV in Tornado.

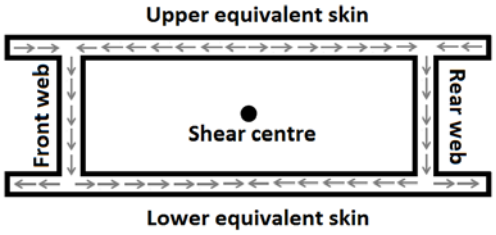

Figure 4. The shear flow in the equivalent rectangular wingbox section.

Dimensional forms of moments (roll and yaw) are used because the aerodynamic loads and the wing structure do not scale in the same way. This might significantly impact the aeroelastic behaviour of the ATW and limit its applicability and success to small scale vehicles.

3.3 Structures

The wingbox is modelled as a thin-wall Euler-Bernoulli beam with torsion. The wingbox is discretised into elements, and conceptual sizing of its various components is performed locally along the span using an ultimate load factor[20]. The structural properties of the elements are then computed. Throughout the sizing process, the webs are assumed to be located at their original positions corresponding to the maximum torsional stiffness as shown in Figure 1(b).

The wingbox is assumed to be made of Aluminium 2024-T3. An ultimate load factor of 6g and a safety factor of 1·5 are used. This results in an equivalent skin thickness (covers + stringers) varying between 1mm at the root to 0·4mm at the tip, and spar web thickness varying between 0·5mm at the root to 0·15mm at the tip. For the sake of simplicity, an equivalent skin thickness (covers + stringers) of 1mm and a web thickness of 0·4mm are selected throughout the wingbox span in this analysis.

3.3.1 Shear centre position

A design module to estimate the shear centre position for different web positions is developed. The wingbox is modelled as an equivalent rectangular cross-section as shown in Fig. 4. The effective depth of the equivalent section is assumed to be 8% of the local wing chord. The shear centre is defined as the point in the cross-section through which shear loads produce no twisting[24]. Therefore its position is estimated by equating the moment produced by the overall shear force acting on the cross-section and the total moment produced by the shear forces in the individual members of the wingbox (equivalent skins and webs). The individual shear forces in each member are obtained by integrating the shear flow in those members.

3.4 Finite Element (FE)

The FE models the wingbox as an Euler-Bernoulli beam with torsion. It rearranges the spanwise aerodynamic loads into equivalent loads at the nodes of each element (defined by the Structural Model). The inertia and stiffness matrices of each element are computed and transformed from

their local co-ordinates to the wing coordinates (global) and then they are assembled to give the wing inertia and stiffness matrices [**M**] and [**K**] respectively.

Six degrees of freedom are considered per node. The nodal deflections are then computed and fed back into Tornado to modify the wing vortex lattice geometry and to generate new aerodynamic loads. This process continues until the aeroelastic loop converges and equilibrium between aerodynamic loads and wing deflection is established.

3.5 Flutter and divergence

Flutter (bending-torsion) and divergence checks are also included in this study. They are based on the finite element approach coupled with Theodorsen's unsteady aerodynamic theory[25,26]. The wing's stiffness and inertia matrices, computed using the FE model discussed above, are simplified so that only three degrees of freedom per node are considered. These degrees of freedom correspond to plunge, twist, and bending rotation. For unsteady aerodynamics, the lift force per unit span (L') on the aerodynamic centre and the pitching moment (M'_o) per unit span at the aerodynamic centre can be expressed as;

$$L' = \frac{\pi\rho c^2}{4}\left[-\ddot{w} + V\dot{\theta} + \frac{c}{4}\ddot{\theta}\right] + \pi\rho V c C(k)\left[-\dot{w} + V\theta + \frac{c}{2}\dot{\theta}\right] \quad \ldots (2)$$

$$M'_o = \frac{\pi\rho c^2}{4}\left[\frac{c}{4}\ddot{w} - \frac{Vc}{2}\dot{\theta} - \frac{3}{32}c^2\ddot{\theta}\right] \quad \ldots (3)$$

where ρ is the air density, U is the airspeed, c is the wing chord, w is vertical the plunge displacement, θ is the twist angle, and $C(k)$ is the Theodorsen's transfer function that accounts for attenuation of lift amplitude and phase lag in lift response due to sinusoidal motion. In order to obtain the lift and moment per unit span in time domain, a low-dimensional state-space representation of the Theodorsen's unsteady aerodynamic theory was employed. This low dimensional representation employs a Pade approximation of Theodorsen's transfer function. Ajaj *et al*[26] provides more details about the reduced order, state-space representation of the classical unsteady aerodynamics. The nodal forces and moments are obtained by integrating the lift and pitching moment per unit span over half the length of each node's adjacent elements. Then, the governing equations of motion of the wing can be arranged as:

$$([\mathbf{M}] - [\mathbf{A}])\{\ddot{\mathbf{q}}\} + ([\mathbf{C}] - [\mathbf{B}])\{\dot{\mathbf{q}}\} + ([\mathbf{K}] - [\mathbf{D}])\{\mathbf{q}\} = 0 \quad \ldots (4)$$

where [**A**] is the aerodynamic inertia matrix, [**B**] is the aerodynamic damping matrix, [**D**] is the aerodynamic inertia matrix, [**C**] is the structural damping matrix which is set to zero in this study, and {**q**} is the vector of the degrees of freedom. Then the equations of motion are arranged in state-space form as follows:

$$\begin{Bmatrix}\dot{\mathbf{q}}\\ \ddot{\mathbf{q}}\end{Bmatrix} - [\mathbf{Q}]\begin{Bmatrix}\mathbf{q}\\ \dot{\mathbf{q}}\end{Bmatrix} = 0 \quad \ldots (5)$$

From the eigenvalues of the [**Q**] matrix, the flutter and divergence speeds can be estimated. To obtain the flutter speed, the flight speed is increased gradually until the real part of one of the eigenvalues of [**Q**] becomes positive. At this point, flutter is initiated and the speed at which this

occurs is the flutter speed. Similarly for divergence speed, the damping matrices are set to zero, and the flight speed is increased gradually until one of the real eigenvalues of [**Q**] becomes positive. At this point, divergence is initiated and the speed at which this occurs is the divergence speed.

4.0 PERFORMANCE STUDY

In this analysis, some of the performance benefits that can be achieved with the ATW concept are assessed. The objective is to maximise the aerodynamic efficiency factor (lift-to-drag ratio) at the start of cruise flight point. Each semi-span of the wing is split into five equal partitions, and in each wing partition the ATW concept is employed. The partitions are assumed to be connected by bulky ribs that can transfer the loads between the wing partitions and maintain smooth load path along the wing.

Two cases are examined here at the start of cruise flight point where the operating conditions are listed in Table 2. In the first case, the wing initial configuration has no geometric twist while in the second case the wing initial configuration has built-in geometric twist.

Table 2
Operating conditions at cruise

Flight parameters	Values
Speed	$60 ms^{-1}$
Altitude	10,000ft
Air density	$0{\cdot}905 kg/m^3$

4.1 Without geometric twist

The wing initial configuration has no geometric pre-twist, and the improvement in the aerodynamic efficiency is to be achieved from the aeroelastic twist induced by the airflow on the wing due to the change in torsional stiffness from the ATW concept. Table 3 summarises the optimisation problem:

Table 3
Problem definition

Objective	**Maximise (*L/D*)**
Variables	x_{fw_i} x_{rw_i} $i = 1, 2, \ldots, 5$
Constraints	$0 \le x_{fi} \le 30$ $0 \le x_{r_i} \le 30$ altitude =10,000ft $L = W$ $U_{div} \le 1{\cdot}25\ U_{dd}$ $U_f \le 1{\cdot}25\ U_{dd}$

where x_{fw_i} is the position of front web for the i^{th} partition and x_{rw_i} is the position of rear web for the ith partition. Figure 5 shows the wing configuration after the ATW is embedded in each of the five partitions. Since the wing and webs positions are symmetric (with respect to the aircraft

centreline) the total number of design variables becomes 10. The optimiser starts generating different individuals with different web configurations. For each individual configuration, GA runs are performed between flight speeds of 20ms^{-1} to 60ms^{-1} to find the minimum drag speed. Once the minimum drag speed is achieved, the optimiser assesses the aerodynamic efficiency and generates a new individual. The same process is repeated until the optimum configuration is found.

The baseline UAV has an aerodynamic efficiency factor of 20. After a GA run of 50 Generations, with 50 Individuals, the optimiser converges and finds the optimum webs distribution. This optimum configuration has an aerodynamic efficiency factor of 20 which is equal to the baseline efficiency factor. This indicates that no improvement was achieved. The optimum webs distribution is listed in Table 4 (Optimum no twist). Therefore when the ATW wing concept was employed without geometric pre-twist, no performance improvements were achieved.

The optimum web distribution in Table 4 shows that for partitions 1, 2, 3, and 4, the optimiser tends to minimise the movement of both spar webs in order to minimise the aeroelastic twist. On the other hand, for partition 5, the optimiser keeps the front web almost fixed and shifts the rear web close to the allowable limit (30%). This is because as the rear web moves forward, the moment arm (distance between aerodynamic centre and shear centre) will significantly reduce and hence the tip aeroelastic twist will be very small. In order to investigate the physical reason behind this conclusion, a variety of critical web distributions were considered. These are listed in Table 4.

Table 4
Webs distributions cases studied

Cases	Webs	P1	P2	P3	P4	P5
Stationary	**F**	0	0	0	0	0
webs	**R**	0	0	0	0	0
Front	**F**	30	30	30	30	30
webs	**R**	0	0	0	0	0
Rear	**F**	0	0	0	0	0
webs	**R**	30	30	30	30	30
Both	**F**	15	15	15	15	15
webs	**R**	15	15	15	15	15
Optimum	**F**	4	1	2	4	0
(no twist)	**R**	0	3	1	1	28
Optimum	**F**	6	0	7	5	3
(with twist)	**R**	3	6	13	14	13

Case 1 (Stationary webs) corresponds to the case where all the webs are fixed in their original locations. Case 2 (Front webs) corresponds to the movement of all the front webs rearward to 30% of wingbox chord while keeping the rear fixed in their original position. Case 3 (Rear webs) corresponds to the movement of all the rear webs forward to 30% of wingbox chord while keeping the front fixed in their original position. Finally, Case 4 (Both webs) corresponds to the movement of all the front webs rearward and the rear webs forward to 15% of wingbox chord. The aeroelastic twist, local incidence

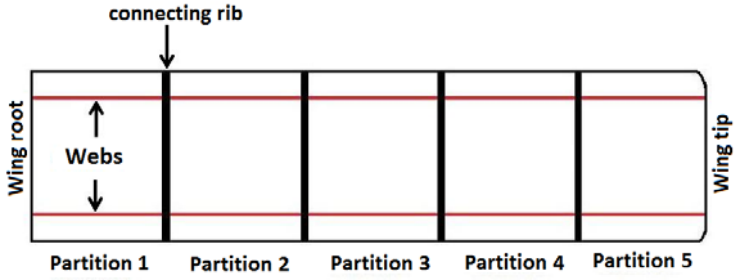

Figure 5. The multi-partition ATW concept without geometric pre-twist.

and drag polar are examined for each of the cases as shown in Figs 6, 7, and 8 respectively. Figure 6 shows that the aeroelastic twist for the optimum webs positions is very similar to that achieved for the stationary webs case. On the other hand, the aeroelastic twists for cases 2, 3, and 4 are much higher. The highest aeroelastic twist is achieved with case 2 where the front webs moves to the extreme positions while the rear webs are kept fixed. The reason for this is that with the movement of the front webs alone, the torsional stiffness reduces and the moment arm between the aerodynamic centre and shear centre also increases.

Figure 7 shows the spanwise local incidence (aeroelastic twist and angle-of-attack) for the different cases. The differences between the curves are of the order of 0·005 radians which is relatively small to provide any changes in the overall spanwise lift distribution. It should be noted

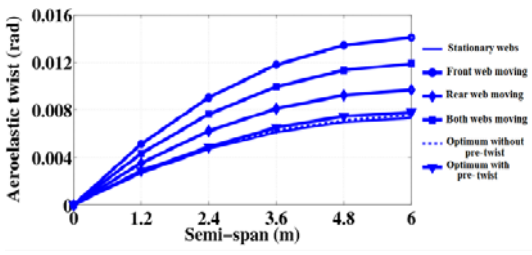

Figure 6. The spanwise aeroelastic twist of the ATW multi-partitions wing.

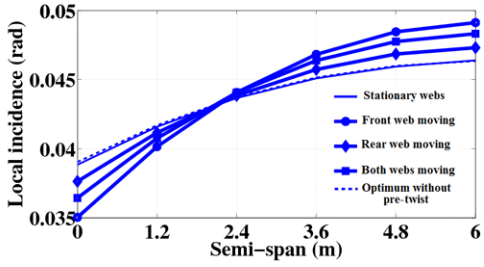

Figure 7. The spanwise incidence of the ATW multi-partition wing.

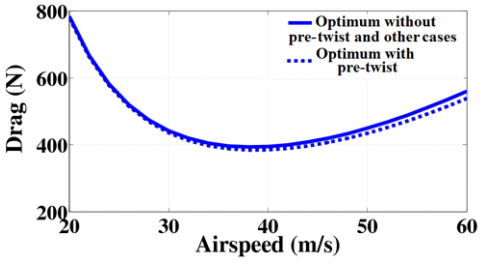

Figure 8. The drag polar of the ATW multi-partition wing.

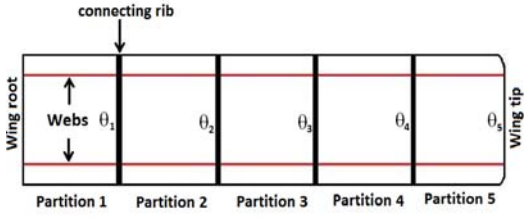

Figure 9. The multi-partition ATW concept with geometric pre-twist.

that both case 1 and the optimum configuration have higher local incidence inboard on the wing and smaller incidence outboard when compared to the other cases. This means that to improve the aerodynamic efficiency the optimiser was trying to concentrate the lift inboard on the wing. In figure 7, the small differences in the local incidence between the different cases result in almost no change to the drag polar and the minimum drag speed (38ms^{-1} for all cases) as shown in figure 8.

4.2 With geometric twist

To enhance the benefits of the concept a new set of design variables are added. These new design variables are the geometric (built-in) twists of each of the wing partitions. This gives more flexibility to control the spanwise lift distribution using both the geometric and aeroelastic twists. Table 5 shows the new optimisation problem:

where θ_i twist at the tip end of the i^{th} partition. Figure 10 shows the wing configuration after the new set of design variables has been added.

The twist at the root of the wing is set to be zero as this belongs to the partition inside the fuselage. A GA run of 100 generations, with 75 individuals, was selected because the number of design variables has increased from 10 for the case with no twist up to 15 in this case. An improvement in the aerodynamic efficiency factor of 2·5% was achieved, yielding an aerodynamic efficiency factor of 20·5. The overall local incidence (angle of attack plus geometric twist plus aeroelastic twist) is shown in Fig. 10.

Figure 6 shows that the spanwise aeroelastic twist of the optimum configuration with pre-twist is slightly higher than that of the optimum without pre-twist. Figure 10 shows that when the geometric twist is varied, the optimum spanwise local incidence becomes significantly different to the case where only the aeroelastic twist is varied. The incidence has its highest values (0·062 radians) at the root and starts to drop over the first partition until it reaches 0·040 radians. Then it starts to increase until it reaches 0·050 radians. Again, it starts dropping gradually over partitions 3 and 4. The local incidence remains almost constant over partition 5. This results in a slight drop of the drag polar curve, as shown in Figure 8, providing a 2·5% increase in the aerodynamic efficiency.

Table 5
Problem definition

Objective	**Maximise (*L/D*)**
Variables	x_{fwi} x_{rwi} θ_i $i = 1, 2, \ldots, 5$
	$0 \le x_{fi} \le 30$ $0 \le x_{ri} \le 30$ $-2{\cdot}85° \le \theta_i \le 2{\cdot}85°$
Constraints	altitude =10,000ft $L = W$ $U_{div} \le 1{\cdot}25\ U_{dd}$ $U_{fr} \le 1{\cdot}25\ U_{dd}$

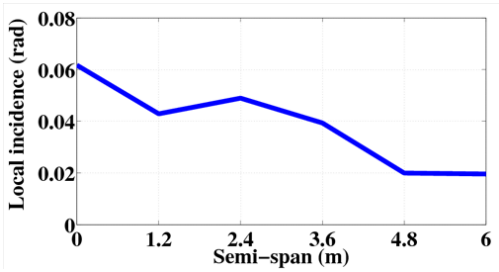

Figure 10. The spanwise local incidence of the multi-partition ATW with geometric pre-twist.

5.0 ROLL CONTROL

The main objective is to achieve roll control without the need for conventional ailerons. The roll control is achieved by changing the web locations on one side of the wing only. The aeroelastic twist induced will increase the lift on one side of the wing leading to a large rolling moment. At the start of cruise, an aileron deflection of 5° generates a rolling moment (*RM*) of L_r = 8kNm and a yawing moment (*YM*) of N = 745Nm, resulting in an *RM* to *YM* ratio of 10·74. The objective in this study is to maximise the ratio of *RM* to *YM* (rolling efficiency factor) while meeting other design constraints. The optimisation problem is summarised in Table 6.

Table 6
Problem definition

Objective	**Maximise (*L/D*)**
Variables	x_{fw_i} x_{rw_i} $i = 1, 2, \ldots, 5$
Constraints	$0 \le x_{fw_i} \le 40$ $0 \le x_{rw_i} \le 40$ $x_{rw_i} + x_{fw_i} \le 70$ $8\text{kNm} \le L_r \le 10\text{kNm}$ $N \le 745\text{Nm}$ altitude =10,000ft $U_{div} \le 1{\cdot}25\ U_{dd}$ $U_{fr} \le 1{\cdot}25\ U_{dd}$

A GA run of 250 generations with 500 individuals has been selected. A rolling moment of L_r = 8kNm and a yawing moment N = 478Nm were achieved. This resulted in an *RM* to *YM* ratio of 16·73. For a symmetric aileron deflection to achieve the same rolling moment resulted in a *RM* to *YW* ratio of 10·74. This indicates that the *ATW* provides a more useful rolling device as it can minimise the associated adverse yawing moment by up to 35%, which would result in much lower drag overall especially at low speed flight phases where induced drag is dominant. The optimum web configuration from the GA is listed in Table 7.

Table 7
Optimum webs positions to maximise rolling efficiency without root constraints

Webs	P1	P2	P3	P4	P5
Front	39	4	0	0	0
Rear	31	0	0	0	0

A tip twist of 2·1 degrees was achieved. It should be noted that the optimiser tries to move both webs as close as possible to the maximum permissible value in partition 1 at the wing root. Furthermore, the optimiser tends to minimise the movement of the spar webs in partitions 2, 3, 4, and 5. Figure 11 shows the spanwise aeroelastic twist. The change in aeroelastic twist is the largest over partition 1 and then it settles down and starts to drop gradually until it becomes

negligible over partition 5. Therefore to maximise the *RM* to *YM* ratio, the optimiser shifts the lift distribution (maximum aeroelastic twist) inboard although this results in a smaller rolling arm (smaller yawing moment). By examining the optimum web positions, the optimiser tries to minimise the torsional stiffness as much as possible around the root section. In practice, this is difficult to achieve due to the various functions of the wing root and the conflicting design requirements, in addition to the large drops in flutter and divergence speeds. Therefore to minimise the movement of the webs in the wing root partition, a new constraint is added yielding a new optimisation problem which is summarised in Table 8.

Table 8
Problem definition

Objective	**Maximise (*L/D*)**
Variables	x_{fwi} x_{rwi} $i = 1, 2, \ldots, 5$
Constraints	$0 \leq x_{fwi} \leq 40$ $0 \leq x_{rwi} \leq 40$ $x_{rwi} + x_{fwi} \leq 70$ $x_{fwi} \leq 20$ $x_{rwi} \leq 20$ $8\text{kNm} \leq L_r \leq 10\text{kNm}$ $N \leq 745\text{Nm}$ altitude =10,000ft $U_{div} \leq 1{\cdot}25\ U_{dd}$ $U_{fr} \leq 1{\cdot}25\ U_{dd}$

An *RM* to *YM* ratio of 14·95 was achieved. A rolling moment L_r = 8kNm and a yawing moment of N = 535Nm were achieved. The adverse yawing moment has reduced by 28%. A tip twist of 2·4° was achieved. The optimum web configuration from the GA is listed in Table 9.

Table 9
Optimum webs positions to maximise rolling efficiency with root constraints

Webs	P1	P2	P3	P4	P5
Front	19	37	29	32	1
Rear	20	34	0	0	0

The optimiser drives the webs in partitions 1 and 2 to the maximum permissible value. For partitions 3 and 4 the optimiser drives the front web rearward and keeps the rear fixed in its original position, while it fixes both webs in their original positions for partition 5. Figure 11 shows the spanwise aeroelastic twist to maximise the *RM* to *YM* ratio where the movements of the root's webs are constrained. The largest change in the twist occurs over partition 2. Then the rate of twist starts to settle down and becomes almost zero over partition 5. The tip twist achieved with the root constraint is higher than the case without constraint. Furthermore the lift distribution is constrained on the outboard of the wing when compared to the case where there is no root constraint.

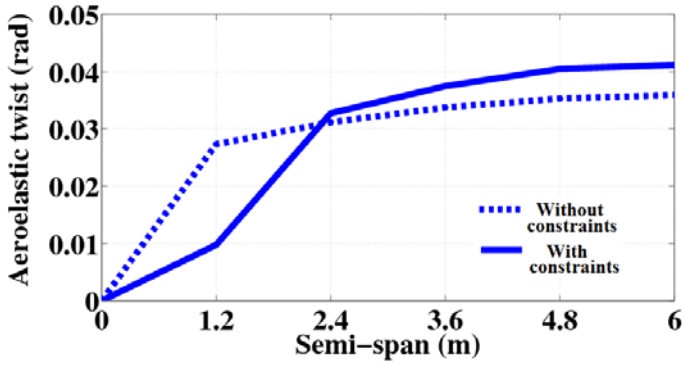

Figure 11. Spanwise aeroelastic twist over the ATW multi-partition wing to maximise rolling efficiency.

6.0 CONCLUSIONS

Two multidisciplinary design optimisation (MDO) studies have been performed. The first investigated the use of the Adaptive Torsion Wing (ATW) concept in the wing of a representative UAV to enhance its aerodynamic efficiency. The ATW concept was not able to provide any improvement in the aerodynamic efficiency of the air-vehicle. However, when the ATW is considered with variable geometric twist, a 2·5% improvement in the aerodynamic efficiency was achieved. The main reason for this is that the ATW is only capable of providing a positively increasing aeroelastic twist (pitching up) along the wing span, and hence the spanwise lift distribution moves outboard resulting in a higher induced drag (lower Oswald efficiency factor).

By introducing variable geometric twist to the ATW, the wing flexibility increases while the lift is concentrated inboard providing a drop in the overall drag. The second study investigated the use of the ATW to provide roll control and replace the ailerons. The ATW showed superior behaviour when compared to conventional ailerons as it was capable of providing the required rolling moment with a smaller adverse yawing moment.

Furthermore, the ATW can be used to allow shorter take-off and landing by increasing the available lift at both flight segments. This implies that when the ATW is employed into the wing to replace the ailerons, it can be used as a flap at the same time. It should be noted that this analysis does not account for the change in wing weight when the ATW is employed due to lack of knowledge on the design and manufacturing of such a concept.

7.0 FUTURE WORK

One of the problems associated with designing morphing structures is that existing aircraft structures have been already optimised over history. This adds many constraints on any morphing concept regardless of its novelty. With the ATW concept, there are several issues to be addressed. During the actuation of the webs, the contact between the skins and the webs must be maintained to ensure that the closed wingbox section is preserved. This requires a large number of connections similar to the ribs to transfer the load between the webs and skins. Furthermore the ribs must be thicker to maintain the load path across the wingbox when the webs of a particular partition are actuated. If the wingbox is designed to carry fuel, then there must be holes in the webs to allow the fuel to move from the closed wingbox to the open wingbox (between the leading edge and the new web position). The rear web is

less effective than the front web in providing large aeroelastic twist, and hence the rear web may be fixed in any physical prototype. The authors are investigating the dynamical modelling of the concept which allows the actuation power required to drive the webs to be estimated. Finally, the weight of the concept may be the main design driver, depending on the scale and mission of the vehicle. The ATW concept has proved to be beneficial only for control purposes, and thus its weight must be equal to or smaller than the weight of conventional control surfaces, unless stealth is the design driver.

ACKNOWLEDGMENTS

The research leading to these results has received funding from the European Research Council under the European Union's Seventh Framework Programme (FP/2007-2013) / ERC Grant Agreement n. [247045].

REFERENCES

1. FRISWELL, M.I. and INMAN, D.J. Morphing Concepts for UAVs, 21st Bristol UAV Systems Conference, April 2006.
2. KUZMINA, S., AMIRYANTS, G., SCHWEIGER, J., COOPER, J., AMPRIKIDIS, M. and SENSBERG, O. 2002 Review and Outlook on Active and Passive Aeroelastic Design Concept for Future Aircraft. ICAS 2002 Congress, 8-13 September, Toronto, Canada, ICAS, 432, pp 1–10.
3. SCHWEIGER, J. and SULEMAN, A. The European Research Project – Active Aeroelastic Structures CEAS Int Forum on Aeroelasticity and Structural Dynamics, 2003.
4. SIMPSON J., ANGUITA-DELGADO L., KAWIESKI G., NILSSON B., VACCARO V. and KAWIECKI, G. Review of European Research Project Active Aeroelastic Aircraft Structures (3AS), European Conference for Aerospace Sciences (EUCASS), 2005, Moscow, Russia.
5. MILLER, G.D. Active Flexible Wing (AFW) Technology, Rockwell International North American Aircraft Operations, 1988, Los Angeles, CA, USA, Report: AFWAL-TR-87-3096.
6. CLARKE, R., ALLEN, M.J., DIBLEY, R.P., GERA, J. and HODGKINSON, J. Flight Test of the F/A-18 Active Aeroelastic Wing Airplane, AIAA Atmospheric Flight Mechanics Conference and Exhibit, San Francisco, CA, AIAA 2005-6316, 2005.
7. PENDLETON, E.W., BESSETTE, D., FIELD, P.B., MILLER, G.D. and GRIFFIN, K.E. Active aeroelastic wing flight research program: technical program and model analytical development, *J Aircraft*, 2000, **37**, (4), pp 554-561, doi: 10.2514/2.2654.
8. GRIFFIN, K.E. and HOPKINS, M.A. Smart stiffness for improved roll control, *J Aircraft*, *Engineering Notes*, 1997, **34**, (3), pp 445-447.
9. CHEN, P.C., SARHADDI, D., JHA, R., LIU, D.D., GRIFFIN, K. and YURKOVICH, R. Variable stiffness spar approach for aircraft manoeuvre enhancement using ASTROS, September-October 2000, *J Aircraft*, **37**, (5).
10. NAM, C., CHEN, P.C., SARHADDI, D., LIU, D., GRIFFIN, K. and YURKOVICH, R. Torsion-Free Wing Concept for Aircraft Maneuver Enhancement, 2000, AIAA/ASME/ASCE/AHS/ASC Structures, Structural Dynamics and Materials Conference, Atlanta, GA, USA, AIAA 2000-1620.
11. FLORANCE, J.R., HEEG, J., SPAIN, C.V. and LIVELY, P.S. Variable Stiffness Spar Wind-Tunnel Modal Development and Testing, 45th AIAA/ASME/ASCE/AHS/ASC/ Structures, Structural Dynamics and Materials Conference, Palm Springs, California, USA, AIAA 2004-1588, 2004.
12. AMPRIKIDIS, M., COOPER, J.E. and SENSBURG, O. 2004. Development of an Adaptive Stiffness All-Moving Vertical Tail, 45th AIAA/ASME/ASCE/AHS/ASC Structures, Structural Dynamics, and Materials Conference, Palm Spring, California, USA, AIAA 2004-1883.
13. COOPER, J.E., AMPRIKIDIS, M., AMEDURI, S., CONCILIO, A., SAN MILLAN, J. and CASTANON, M. Adaptive Stiffness Systems for an Active All-Moving Vertical Tail, European Conference for Aerospace Sciences (EUCASS) 4-7th July, 2005, Moscow, Russia.
14. COOPER, J.E. Adaptive stiffness structures for air vehicle drag reduction. In Multifunctional Structures/Integration of Sensors and Antennas (pp 15-1-15-12). Meeting Proceedings RTO-MP-AVT-141, Paper 15, Nueuilly-sur-Seine, France: RTO, 2006.

15. COOPER, J.E. Towards the Optimisation of Adaptive Aeroelastic Structures, School of Mechanical, Aerospace and Civil Engineering, University of Manchester, UK, 2006.
16. HODIGERE-SIDDARAMAIAH, V. and COOPER, J.E. 2006. On the Use of Adaptive Internal Structures to Optimise Wing Aerodynamics Distribution, 47th AIAA/ASME/ASCE/AHS/ASC Structures, Structural Dynamics, and Materials Conference, Newport, Rhode Island, USA, AIAA 2006-2131.
17. AJAJ, R.M., FRISWELL, M.I., DETTMER, W.G., ALLEGRI, G. and ISIKVEREN, A.T. Conceptual Modelling of an Adaptive Torsion Structure, 52nd AIAA/ASME/ASCE/AHS/ASC Structures, Structural Dynamics and Materials Conference, Denver, Colorado, USA, AIAA-2011-1883, 2011.
18. AJAJ, R.M., FRISWELL, M.I., DETTMER, W.G., ALLEGRI, G. and ISIKVEREN, A.T. Roll Control of a UAV Using an Adaptive Torsion Structure, 52nd AIAA/ASME/ASCE/AHS/ASC Structures, Structural Dynamics and Materials Conference, Denver, Colorado, USA, AIAA-2011-1883, 2011.
19. SMITH, D.D., ISIKVEREN, A.T., AJAJ, R.M. and FRISWELL, M.I. Multidisciplinary Design Optimisation of an Active Nonplanar Polymorphing Wing, 27th International Congress of the Aeronautical Sciences (ICAS 2010) Nice, France, 19-24 September 2010.
20. AJAJ, R.M., SMITH, D., ISIKVEREN, A.T. and FRISWELL, M.I. A conceptual wing-box weight estimation model for transport aircraft, *Aeronaut J*, Accepted, 2012.
21. CHIPPERFIELD, A.J. and FLEMING, P.J. The Matlab Genetic Algorithm Toolbox, IEE Colloquium on Applied Control Techniques using Matlab, Digest No.1995/014, January 1996.
22. CHIPPERFIELD, A.J., FLEMING, P.J. and FONSECA, C.M. Genetic Algorithm Tools for Control Systems Engineering, Proc.1st Int. Conf. Adaptive Computing in Engineering Design and Control, Plymouth Engineering Design Centre, UK, 1994, 21-22 September, pp 128-133.
23. MELIN, T. A Vortex Lattice MATLAB Implementation for Linear Aerodynamic Wing Applications, Royal Institute of Technology (KTH), December 2000.
24. MEGSON, T.H.G. *Aircraft Structures for Engineering Students*, Chapter 9, Bending, shear and torsion of open and closed, thin-walled beams, pp 276-345, Butterworth-Heinemann, Burlington, USA, 2003.
25. WRIGHT, J.R. and COOPER, J.E. *Introduction to Aircraft Aeroelasticity and Loads*, Chapter 11, Dynamic Aeroelasticity-Flutter, John Wiley & Sons Ltd, 2007.
26. AJAJ, R.M., FRISWELL, M.I., DETTMER, W.G., ALLEGRI, G. and ISIKVEREN, A.T. Dynamic modelling and actuation of the adaptive torsion wing, *J Intelligent Material Systems and Structures* (JIMSS), Accepted, 2012.